Continuous Casting Consortium Report 200902

Analytical Prediction of Funnel Mold Bending Effect and Hot Tearing Susceptibility

Lance C. Hibbeler and Brian G. Thomas

Department of Mechanical Science and Engineering
University of Illinois at Urbana-Champaign
1206 West Green St., Urbana, IL 61801
lhibbel2@illinois.edu

July 17, 2008

ABSTRACT

The thermomechanical behavior of a solidifying steel shell in a continuous casting mold is affected by many phenomena, especially the interaction between the shell and mold. In funnel-shaped molds, the mold causes an extra bending effect in the steel shell due to the significantly different shape of the mold hot face at the bottom of the mold compared with the top. This effect can be quantified accurately with a simple analytical model:

$$\varepsilon_{bending}(z) = \frac{\delta(z)}{r_h(z_{meniscus})} - \frac{\delta(z)}{r_h(z)} = \delta(z)\left(\frac{r_h(z) - r_h(z_{meniscus})}{r_h(z)\, r_h(z_{meniscus})}\right) \quad (1)$$

where $\varepsilon_{bending}$ is the bending strain,

δ is the thickness of the solidified shell, and

r_h is the horizontal radius of the funnel evaluated either at z or $z_{meniscus}$,

z is any distance below the meniscus, such as mold exit.

$z_{meniscus}$ is the distance between the top of the mold and the liquid pool meniscus

Funnel designs naturally should be evaluated according to which produces the best product quality. In this work, the best funnel design depends on the mechanism responsible for forming LFC crack defects. Several distinct mechanisms may cause LFC cracks:

1) LFC and other defects form at the meniscus due to disruption of liquid flux feeding at the meniscus between the shell and mold. Such disruptions can be caused by slag layer solidification due to insufficient fluid flow between the SEN and the mold. Funnel design impacts this mechanism by affecting the space between the SEN and the mold.
2) Hot-tear cracks form between the roots of dendrites at the meniscus (surface) and grow inwards as solidification progresses down the mold. Meniscus problems, such as a finger of mold flux caught between the shell and mold at the meniscus due to level fluctuations are responsible for initiating such cracks. Funnel design impacts this mechanism through its important effect on the flow pattern in the mold, especially in the funnel transition region (curved regions), which is susceptible to the largest level fluctuations.
3) Hot-tear cracks initiate beneath the surface of the shell, due to tensile strain applied across the roots of the dendrites, which concentrates in the inter-dendritic liquid films, and opens up sub-surface cracks. These cracks later propagate through the solidified shell to penetrate the surface, due to overload (see mechanism 4). Funnel design impacts this mechanism because the funnel causes additional mechanical bending strains in the shell.
4) Overload cracks occur at mold exit when the ferrostatic pressure exceeds the rupture strength of local thin spots in the solidifying shell. Previous calculations show that this critical thickness is on the order of 3mm [5]. When a subsurface crack is present, the effective shell thickness is measured from the surface to the root of the crack. Thin spots in the shell can be caused by local gap formation, where the shell is lifted away from the mold or the local slag layer is too thick, or slag feeding is interrupted and replaced with low-conductivity gases. Funnel design and narrow face taper impact this mechanism because they influence gap formation between the mold and the shell.

Of course, a particular LFC cracking problem may be caused by a combination of mechanisms, The best funnel design depends on the mechanism that dominates the formation of those LFCs and other defects. The first step is to determine how funnel design affects each LFC mechanism. This work considers the optimization of funnel design according to several different mechanisms, but focuses on mechanisms 3 and 4, taking into account that thicker funnels are better to avoid mechanism 1.

1. FUNNEL MOLD GEOMETRY

The geometry of a funnel-shaped mold is described by three physical dimensions: the outer funnel width, the inner funnel width, and the funnel crown, as shown in Figure 1. In practice, usually only the crown changes with distance down the mold. Some molds have a zero inner funnel width, which can be taken as a special case of the equations presented in this section.

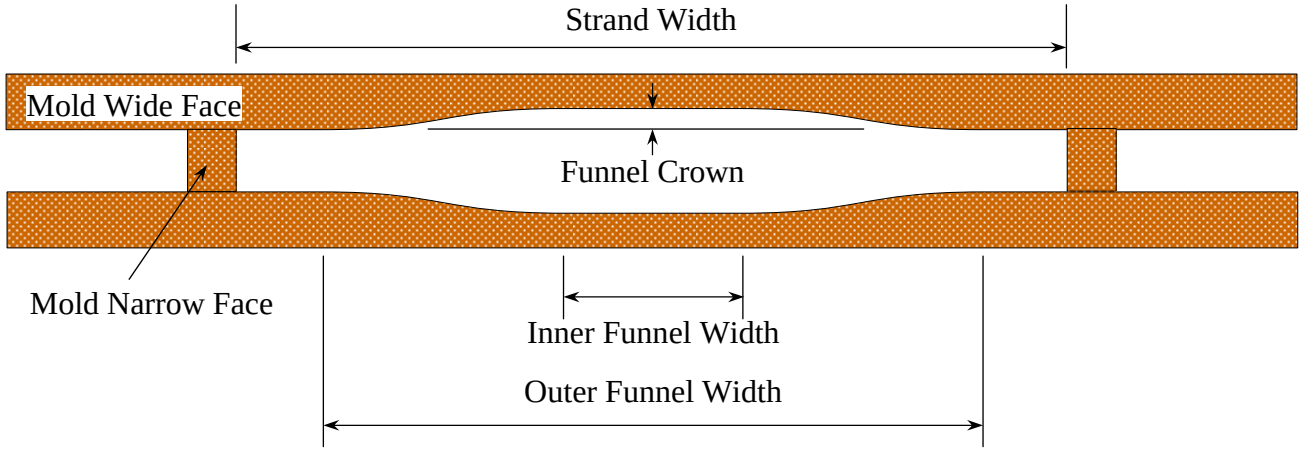

Figure 1. Horizontal Funnel Geometry Terminology (Top View)

The funnel mold has two planes of symmetry, one through the middle of the wide faces and one through the middle of the narrow faces. Their intersection suggests a natural coordinate system for the mold, as shown in Figure 2, with the positive *z*-axis pointing along the casting direction ("into the page"). Consider the quadrant in the horizontal plane bounded by the positive *x*- and *y*- axes. Figure 2 defines the funnel geometry. w_i is half of the inner funnel width, w_o is half of the outer funnel width, w_s is half of the strand width, c is the crown, and t_s is half of the strand width away from the funnel.

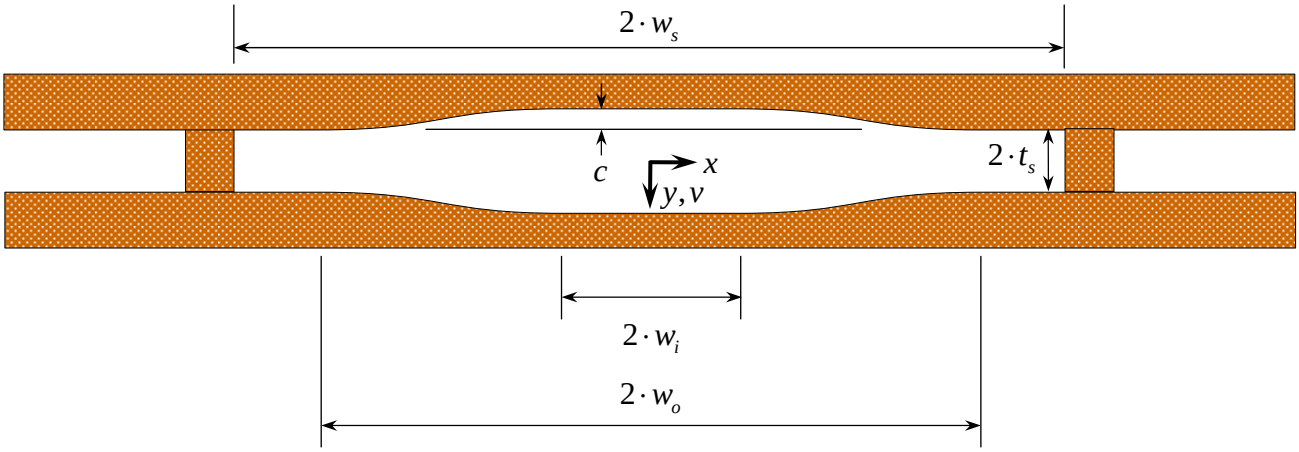

Figure 2. Horizontal Funnel Geometry Variables

The surface of the funnel may be described using laws of geometry, including the Pythagorean Theorem and the law of similar triangles. Note that $w_i < w_o < w_s$. To connect the (x, y) points $(w_i, t_s + c)$ and (w_o, t_s), with a reasonable degree of smoothness (to promote uniform heat transfer between the shell and mold and to facilitate solidification shrinkage with minimal stress), the funnel shape is defined by portions of two circles of equal radius. The "inner curve" radius defines the transition from the "inner flat" region near the mold center to the funnel region, and the "outer curve" radius sweeps from the middle to the end of the funnel region. Geometrically, the inner curve sweeps from point $(w_i, t_s + c)$ to point $\left((w_o + w_i)/2, t_s + c/2\right)$ and is tangent to both the outer curve and the inner flat. The outer curve sweeps from point $\left((w_o + w_i)/2, t_s + c/2\right)$ to point (w_o, t_s) and is tangent to both the inner curve and the "outer flat" region that extends towards the narrow faces, $|x| > w_o$. The radius of both circles is defined by:

$$r_h = \frac{c}{4} + \frac{\left(w_o - w_i\right)^2}{4 \cdot c} \tag{2}$$

The hot face of the wide face depends on r_h according to the following piecewise equation of x:

$$v(x,z) - t_s = \begin{cases} c & 0 \le x \le w_i \\ c - r_h + \sqrt{r_h^2 - \left(x - w_i\right)^2} & w_i \le x \le w_m \\ r_h - \sqrt{r_h^2 - \left(w_o - x\right)^2} & w_m \le x \le w_o \\ 0 & w_o \le x \le w_s \end{cases} \tag{3}$$

Note that c and r_h are both functions of distance down the mold.

The crown may be expressed as a function of distance down the mold, as shown in the vertical section through the center of the wide face given in Figure 4. Figure 4 also identifies some of the other important geometric features of funnel molds, including the "mold length," ℓ_m, which is the distance between the top and bottom of the mold plate, the "funnel length," ℓ_f, which is the distance below the top of the mold that marks the end of the funnel, the crown at the top of the mold c_T, and the crown at the bottom of the mold, c_B. Note that $l_f \le l_m$ and $c_B < c_T$. Although many different shapes can connect the (y, z) points $(t_s + c_T, 0)$ and $(t_s + c_B, \ell_f)$, this work uses a "radiused funnel," a circular arc that is tangent to plane of the vertical mold surface in the lower portion of the funnel that is described by $z > \ell_f$.

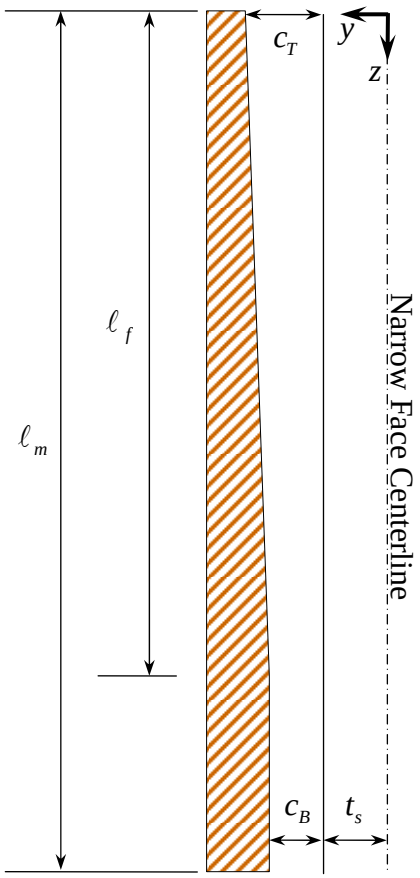

Figure 4. Vertical Mold Geometry Variables (Centerline Slice)

The vertical radius must be calculated before the radiused funnel can be described, and is found with the Pythagorean Theorem:

$$r_v = \frac{c_T - c_B}{2} + \frac{\ell_f^2}{2 \cdot (c_T - c_B)} \tag{4}$$

The piecewise function describing the crown of the radiused funnel is then:

$$c(z) = \begin{cases} c_B + r_v - \sqrt{r_v^2 - (\ell_f - z)^2} & 0 \le z \le \ell_f \\ c_B & \ell_f \le z \le \ell_m \end{cases} \tag{5}$$

Note that both crown functions allow $c_B = 0$ (the funnel disappears entirely at $z = \ell_f$). Figure 5 clarifies the differences between the vertical funnel types. This completes the funnel geometry definition.

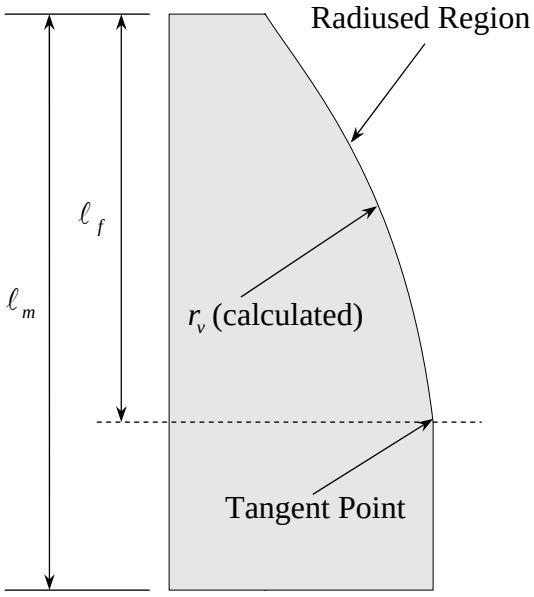

Figure 5. Exaggerated Vertical Funnel Profiles

2. BEAM BENDING MODEL

Continuous casting funnel molds are unique among the various available mold shapes in that the shape of the mold hot face changes *significantly* from the top of the mold to the bottom. All other mold shapes, from simple billets to complicated beam blanks, have only slight changes in shape due to mold taper. The funnel mold hot face shape changes by several centimeters, as given by one of the crown functions described in the previous section. This substantial change in position has consequences on mold taper, and it also bends the solidifying shell as it slides down the mold. The bending effect can be easily modeled by treating the solidifying shell as a beam or plate.

The basis for describing beam and plate bending in solid mechanics [1, 2] is mostly a geometrical argument. Beams are long, slender members of various cross sections where one dimension is much greater than the other two dimensions. A beam is loaded perpendicular to the longitudinal axis, which distinguishes it from a column, which is loaded along the axis. Consider the *initially straight* beam made up of the solidifying steel shell of thickness δ in the y-direction, and width w_s around the mold perimeter as oriented as shown in Figure 6, with the same coordinate system used in Figure 2.

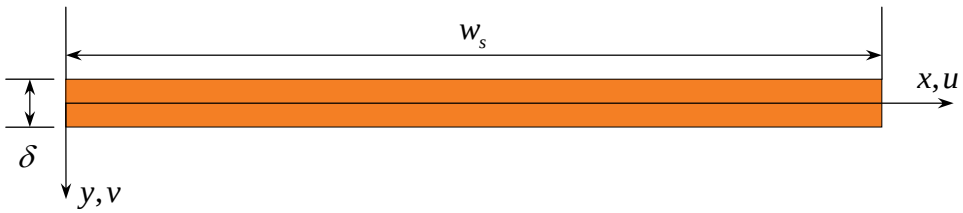

Figure 6. Beam Schematic and Coordinate System

The elementary beam theory employed here considers only σ_x, which is important to the formation of longitudinal cracks. All other stress components are zero ($\sigma_y = \sigma_z = \tau_{xy} = \tau_{xz} = \tau_{yz} = 0$). The "neutral axis" of the beam must be determined as a part of the analysis. It is defined as the region in the cross section where $\sigma_x = 0$, as sketched in Figure 7. The neutral axis experiences no change in length as the beam is deformed, and is located by integrating the stress distribution above and below the neutral axis, and determining constants to make the resultant forces balance:

$$\int_{A_L} \sigma_x dA = \int_{A_U} \sigma_x dA \tag{6}$$

For a linear-elastic material with constant elastic modulus, the typical approach is to assume that axial stress varies linearly with y ($\sigma_x = \eta \cdot y$, where η is a constant), which results in the neutral axis coinciding with the centroidal axis of the cross section (halfway through the thickness of the rectangular cross-section in the example problem). However, in the present analysis of a solidifying steel shell, the assumption of constant elastic modulus is unreasonable. The elastic modulus varies greatly through the shell thickness due to the dependence upon temperature of elastic modulus [3], as shown in Figure 8, and the large temperature gradients across the shell. Thus, the solid material closest to the shell surface is much stronger than the recently-solidified material near the solidification front. This makes the neutral axis only a few millimeters beneath the surface, even when the shell is over a centimeter in thickness.

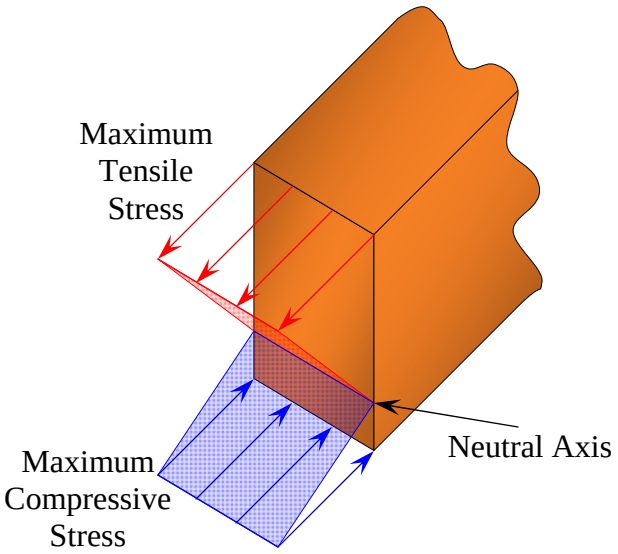

Figure 7. Bending Stress Profile Across Beam Section

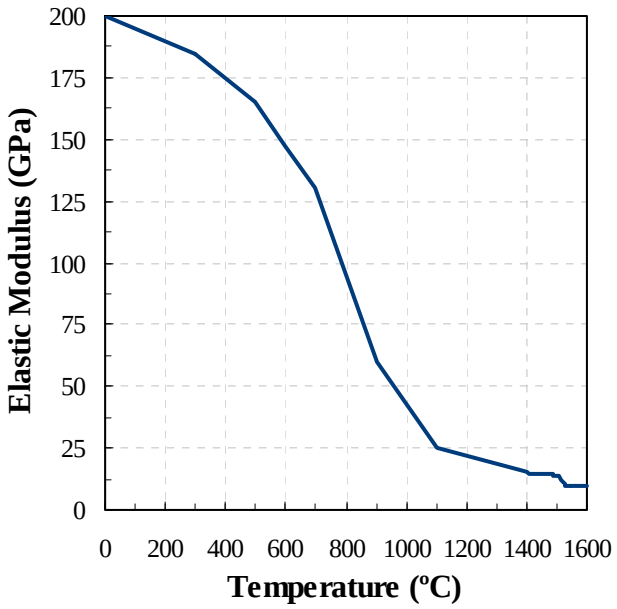

Figure 8. Effect of Temperature on Steel Elastic Modulus

Bending Strain Model

The axial strain through a cross section is determined by the local radius of curvature at a point along the beam axis. Consider a segment of undeformed thickness Δx along the beam axis, as shown in Figure 9a. A line segment on the neutral axis in the segment of the beam will have constant length Δx both before and after deformation. Any other line segment of length Δs at a distance y from the neutral axis will change length to $\Delta s'$ when the beam is bent, as shown in Figure 9b. The axial strain along that line segment is defined as:

$$\varepsilon_x = \lim_{\Delta s \to 0} \frac{\Delta s' - \Delta s}{\Delta s} \tag{7}$$

With only one nonzero stress component, beam theory requires that planar cross-sections remain planar after deformation (no warping). Thus, the beam segment will deform so that its sides rotate to form a defined radius of curvature R, center point C, and subtended angle $\Delta\theta$, as shown in Figure 9b. The arc-length formula gives that the original length of the line segment (initially equal to the segment width Δx) of interest is $\Delta s = R\Delta\theta$, and the deformed length is $\Delta s' = (R - y)\Delta\theta$. Substituting these lengths into the above definition of strain gives:

$$\varepsilon_x = \lim_{\Delta\theta \to 0} \frac{(R - y)\Delta\theta - R\Delta\theta}{R\Delta\theta} \tag{8}$$

which simplifies to:

$$\varepsilon_x = -\frac{y}{R} \tag{9}$$

This axial strain from bending is the total *mechanical* strain, defined as the sum of the elastic and plastic strains, which is equal to the thermal strain subtracted from the total strain in a solidification problem.

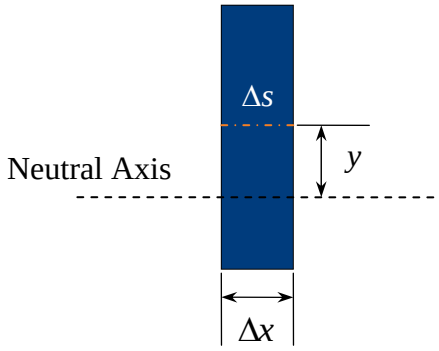

Figure 9a. Undeformed Beam Element

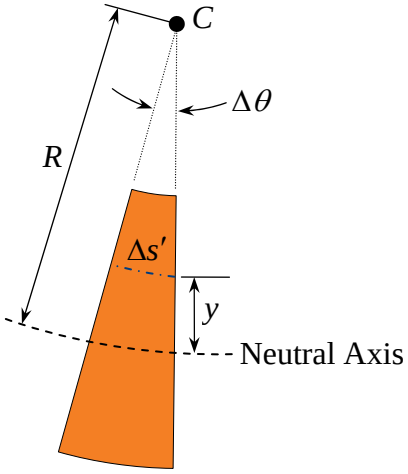

Figure 9b. Deformed Beam Element

This strain in Equation (9) is simply the product of distance from the neutral bending axis and the local radius of curvature. In general, the curvature κ of a line is defined as:

$$\kappa = \frac{1}{R} = \frac{\dfrac{d^2 v}{dx^2}}{\left[1+\left(\dfrac{dv}{dx}\right)^2\right]^{\frac{3}{2}}} \tag{10}$$

where $v(x)$ describes the displacement of the beam in the y-direction. If the slope of v is small, and the curvature can be approximated as $\kappa = d^2 v/dx^2$, but this is not necessary with the funnel mold consisting of actual circles, and the full definition of curvature is maintained, giving: $\kappa = 1/r_h$. The strain developed in bending the beam from the straight configuration to the bent configuration is then:

$$\varepsilon_x = -y \begin{cases} 0 & 0 \le x \le w_i \\ -1/r_h & w_i \le x \le w_m \\ 1/r_h & w_m \le x \le w_o \\ 0 & w_o \le x \le w_s \end{cases} \tag{11}$$

This model can calculate the developing bending strain as a function of distance down the mold. This is accomplished by taking the difference between bending a straight beam to the shape at the meniscus and bending the same straight beam to the shape at some other distance below the top of the mold. The difference represents the bending effect developed from bending a beam with the meniscus shape to the configuration at some other position, as illustrated in Figure 10.

$$\varepsilon_x(z) = \frac{y}{r_h(z_{meniscus})} - \frac{y}{r_h(z)} = y\frac{r_h(z) - r_h(z_{meniscus})}{r_h(z)r_h(z_{meniscus})} \tag{12}$$

If the geometry at given z is such that the horizontal funnel radius is zero, then $\varepsilon_x(z) = y/r(z_{meniscus})$. This simple equation gives the strain of deforming the shell from its original funnel shape at the meniscus to completely flat (at the end of the funnel). Substituting the definition of the horizontal funnel radius, and assuming the entire shell thickness for *y* in Equation (12) gives:

$$\varepsilon_x(z) = \delta \cdot 4 \cdot \frac{\left[c(z_{meniscus}) - c(z)\right]\left[(w_o - w_i)^2 - c(z_{meniscus})c(z)\right]}{\left[c(z)^2 + (w_o - w_i)^2\right]\left[c(z_{meniscus})^2 + (w_o - w_i)^2\right]} \tag{13}$$

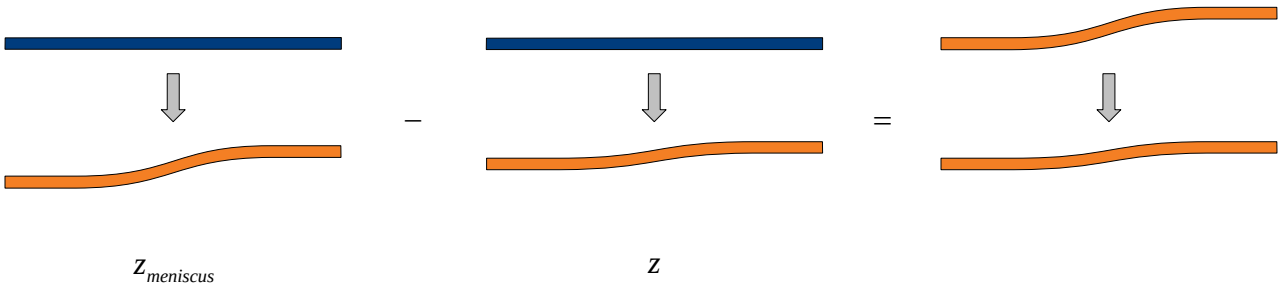

Figure 10. Logic of "Developing" Bending Strain Model

Bending Strain Rate Model

Another quantity of interest is the strain rate at the solidification front. The various cracking criterion available in the literature are expressed in terms of strain and/or strain rate. The analytical model developed here allows the easy calculation of the strain rate by taking the first time derivative of Equation (16) after applying the transformation using the transformation $z = V_C \cdot t + z_{meniscus}$, where V_C is the casting speed and t is time. The shell is assumed to grow as $K\sqrt{t}$, which has both reasonable accuracy and a closed-analytical form:

$$\dot{\varepsilon}_x(z) = \frac{d}{dt}\left[K\sqrt{t}\frac{r_h(z) - r_h(z_{meniscus})}{r_h(z)r_h(z_{meniscus})}\right] = \frac{K}{2\sqrt{t}}\frac{r_h(z) - r_h(z_{meniscus})}{r_h(z)r_h(z_{meniscus})} + \frac{K\sqrt{t}}{r_h(z)^2}\left(\frac{d}{dt}r_h(z)\right) \tag{14}$$

The time derivative of the horizontal radius function for the radiused funnel is given by:

$$\frac{d}{dt}r_h = \begin{cases} \dfrac{(\ell_f - z)\cdot V_C}{4\cdot\sqrt{r_v^2 - (\ell_f - z)^2}}\left[\left(\dfrac{w_o - w_i}{c_B + r_v - \sqrt{r_v^2 - (\ell_f - z)^2}}\right)^2 - 1\right] & 0 \le z \le \ell_f \\ 0 & \ell_f \le z \le \ell_m \end{cases} \tag{15}$$

3. MODEL VALIDATION

To evaluate the accuracy of the bending model, its predictions are compared with the results of a realistic, elastic-viscoplastic two-dimensional coupled thermal-stress finite-element model of the solidifying shell. Note that Equation (1) takes the neutral axis as the surface of the shell, i.e. use the entire shell thickness for y in Equation (12). This assumption introduces an error that evidently is cancelled by the remaining mechanical effect present in the mold: the net solidification shrinkage of the entire shell. Figure 11 shows a plot of the analytical bending strain predicted *at the solidification front* in the inner curve region of a radiused funnel with w_i = 130 mm, w_o = 375 and 475 mm, ℓ_f = 850 mm, c_T = 23.4 mm, and c_B = 8 mm. The lines labeled "numerical model" are from the corresponding finite element simulations, and actually plot the difference between (total strain – thermal strain) at the inner curve and at the center of the wide face (x = 0). Subtracting the center profile removes the effect of solidification from the numerical prediction of the strain, and leaves only the bending effect.

The favorable match between the numerical and analytical prediction clearly identifies the bending effect as the cause of the localized concentrations of mechanical strain in the funnel region, and also shows that this simple bending model can be applied in a parametric study to quantify the effect of different funnel geometries.

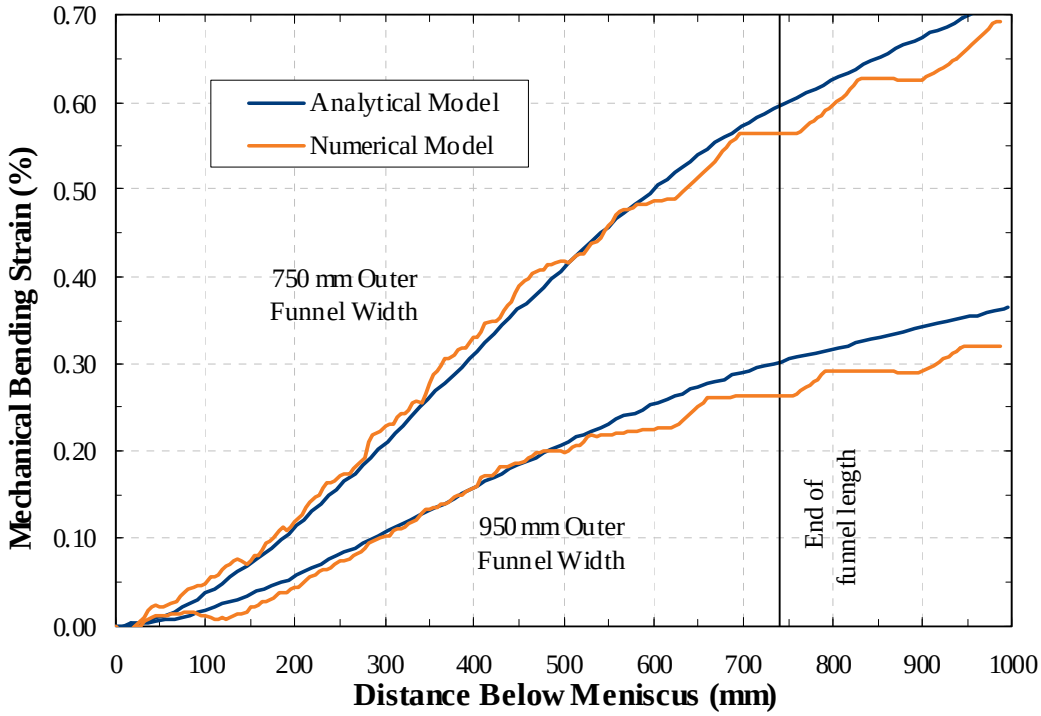

Figure 11. Comparison of Analytical and Numerical Bending Strain Predictions

4. PARAMETRIC STUDIES

The effect of different funnel geometries on bending strain and strain rate are investigated using Equations (13) and (14). Shell thickness at mold exit is taken as δ = 10 mm and nominal funnel mold dimensions are w_i = 130 mm, w_o = 375, ℓ_f = 850 mm, c_T = 23.4 mm, and c_B = 8 mm. Strain rate calculations are based on $V_C = 5.5$ m/min and $K = 2.79$ mm/s$^{1/2}$ to match the shell thickness at mold exit of the two-dimensional finite-element model, which is based on matching heat flux from plant measurements.

Bending Strain at Mold Exit

Attention is first focused on the bending strain developed at mold exit ($z = \ell_m$) in the inner curve region of the funnel, which is the most tensile. Figures 12a and 12b show the effect of changing the funnel geometry, based on Equation 13. With the meniscus 100 mm below the top of the mold, the crown at the meniscus is 20.4 mm. Note the "funnel transition width" $(w_o - w_i)$ is used to reduce the number of parameters in the equation defining the horizontal radius. The bending strain is reduced with wider funnels and shallower crowns, with the limiting value being a parallel-sided wide face, which of course has no bending effect at all. In general, decreasing the crown influences the bending effect more than increasing the funnel transition width.

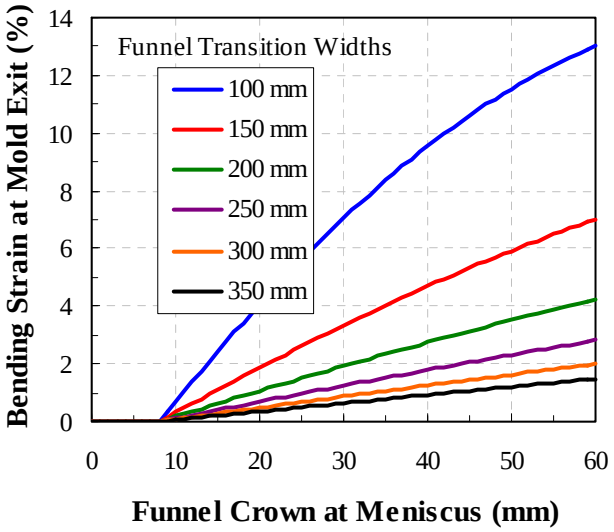

Figure 12a. Effect of Funnel Crown

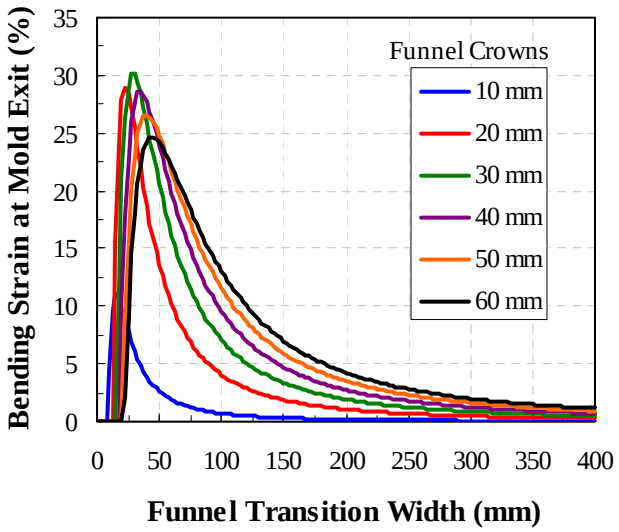

Figure 12b. Effect of Funnel Transition Width

Effect of Funnel Mold Shape

The simple model enables easy comparison between funnels of different geometry. In general, the larger the horizontal radius, the less the bending effect, i.e. the inner funnel width should be minimized, the outer funnel width should be maximized, and the crown should be minimized. Changing the funnel length has little effect on the bending strain, but can significantly change the strain rate profile, which will be discussed later in the context of hot tearing. Figures 13-16 show the results of the analytical model bending strain predictions for different funnel geometries.

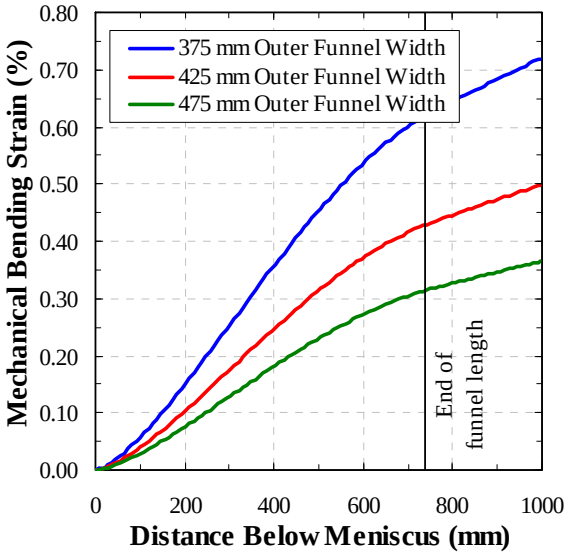

Figure 13a. Effect of Outer Funnel Width on Strain

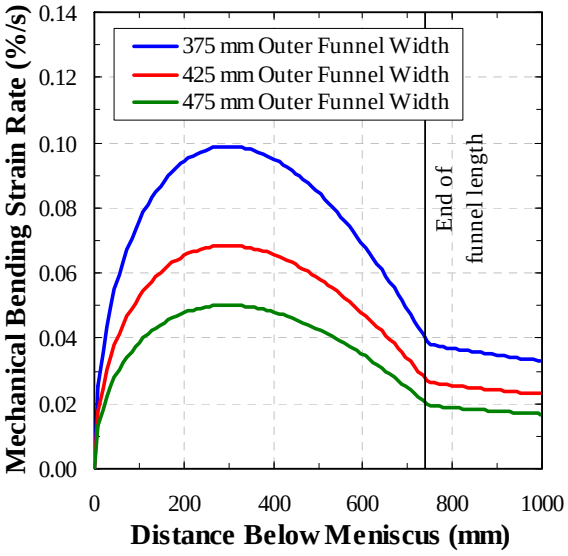

Figure 13b. Effect of Outer Funnel Width on Strain Rate

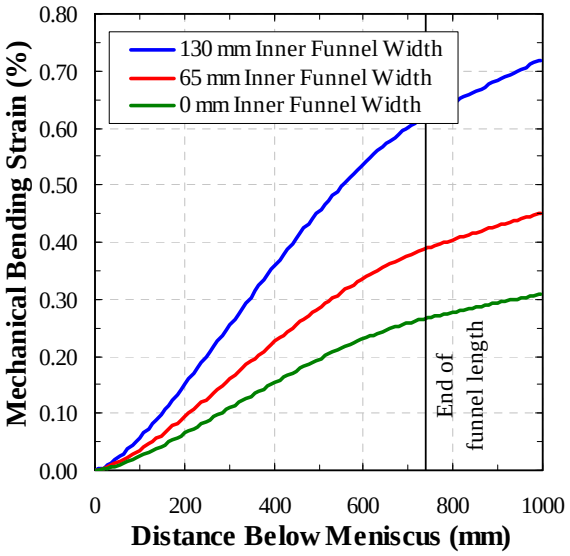

Figure 14a. Effect of Inner Funnel Width on Strain

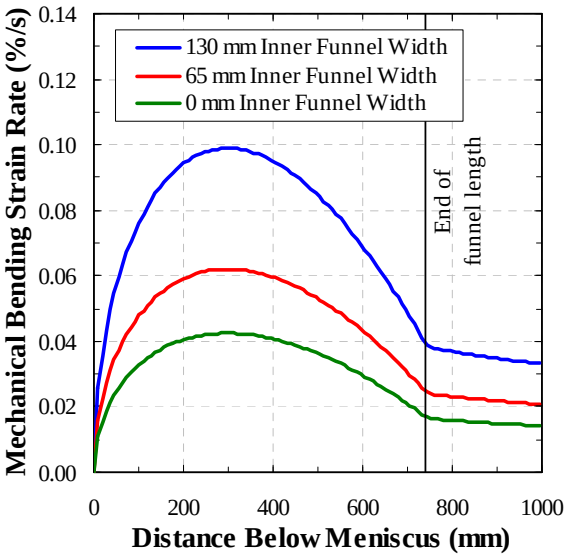

Figure 14b. Effect of Inner Funnel Width on Strain Rate

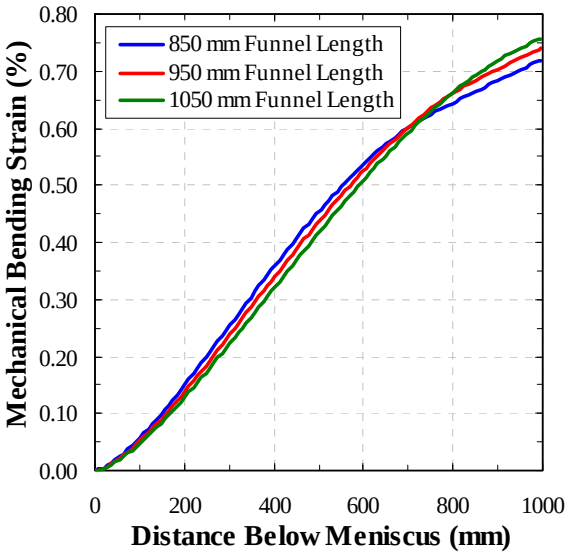

Figure 15a. Effect of Funnel Length on Strain

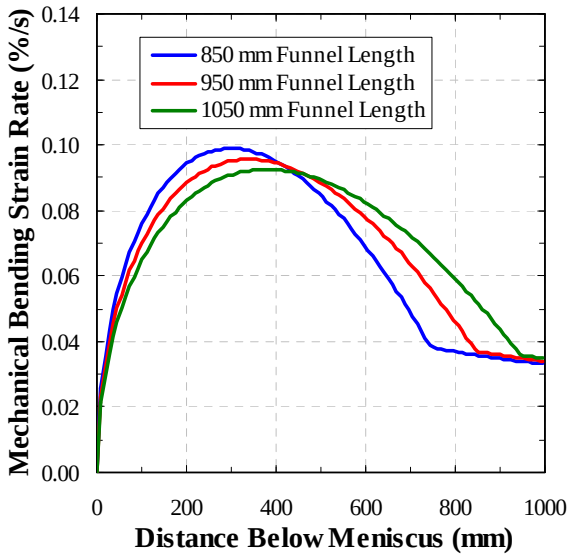

Figure 15b. Effect of Funnel Length on Strain Rate

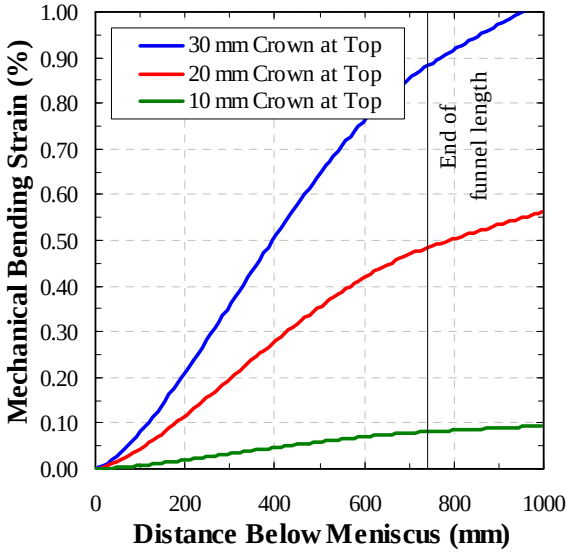

Figure 16a. Effect of Funnel Crown at Top on Strain

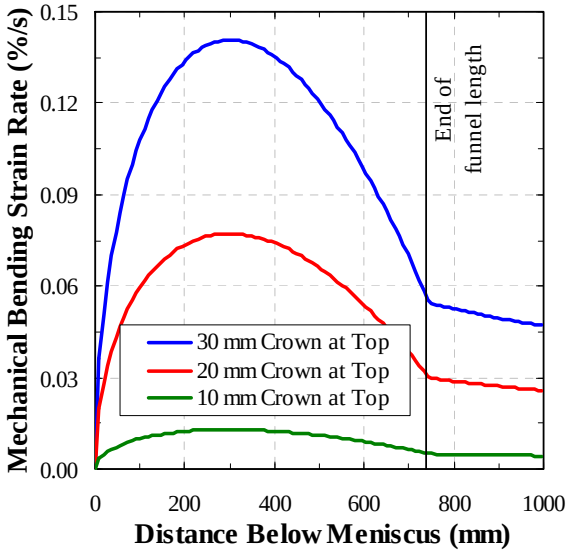

Figure 16b. Effect of Funnel Crown at Top on Strain Rate

5. HOT-TEARING PREDICTIONS

The damage model created by Won [4] that quantitatively predicts hot tears in steels is used here to evaluate the cracking potential caused by the funnel mold. Won's model predicts a critical damage strain in terms of the brittle temperature zone, $\Delta T_B = T(f_s = 99\%) - T(f_s = 90\%)$, and the average inelastic strain rate over the brittle temperature zone:

$$\dot{\varepsilon} = \frac{\varepsilon(f_s = 99\%) - \varepsilon(f_s = 90\%)}{t(f_s = 99\%) - t(f_s = 90\%)} \tag{16}$$

The critical damage strain according to Won is then given by:

$$\varepsilon_c = \frac{0.02821}{\dot{\varepsilon}^{0.3131} \cdot \Delta T_B^{0.8638}} \tag{17}$$

The critical damage strain is compared with the accumulated damage strain in the brittle temperature zone, $\varepsilon_{dmg} = \varepsilon(f_s = 99\%) - \varepsilon(f_s = 90\%)$; cracks will form if the damage strain exceeds the Won critical strain. The ratio of accumulated damage to the critical damage defines the "damage index" $D = \varepsilon_{dmg} / \varepsilon_c$, a single value which facilitates comparison of funnels. Quantities are defined in terms of the fraction solid, and are found by first determining the time at which a given point takes on the given fraction solid, and then calculating the inelastic strain at that time.

Attempting to perform this damage calculation on a two-dimensional model of the funnel mold revealed a great deal of numerical noise in the results, and so motivated by the discussion in the previous section, the results analytical bending model was superimposed upon the results of a one-dimensional slice model of the solidifying shell with realistic properties and heat flux. This model still showed considerable numerical noise, even with 0.06-mm element lengths in the mesh, as shown in Figures 17 and 18. To work around the issue of numerical noise, the steel grade was changed to a higher-carbon steel which has a wider mushy zone and is therefore more crack sensitive.

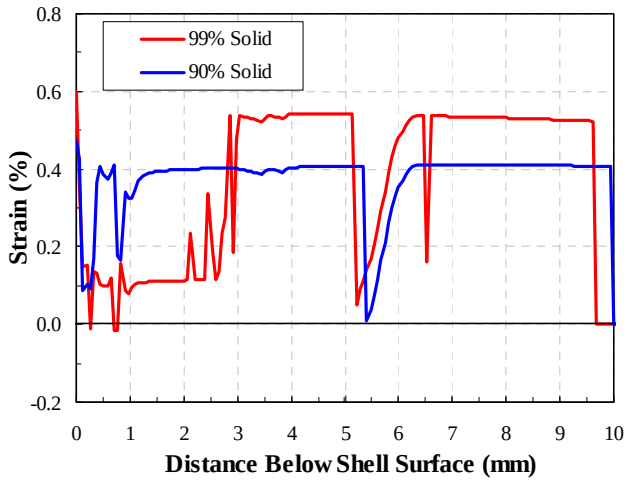

Figure 17. BTZ Strains in a LC Steel

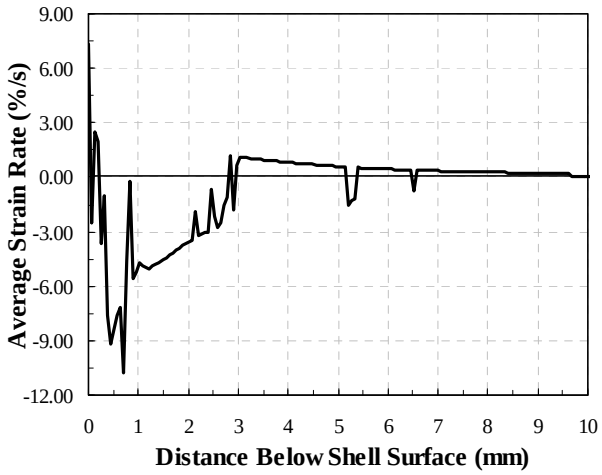

Figure 18. Avg. Inelastic Strain Rate in a LC Steel

Figures 19-22 show the aspects of the damage calculation for a 1 %wt. C steel for the nominal funnel geometry given above, as well as for a wider funnel, a longer funnel, and a parallel mold. The funnel clearly increases the damage strain and decreases the critical strain for an overall increase in damage index, but nevertheless no cracking occurs during normal operation of a funnel mold; some other effect is needed to cause a crack to form.

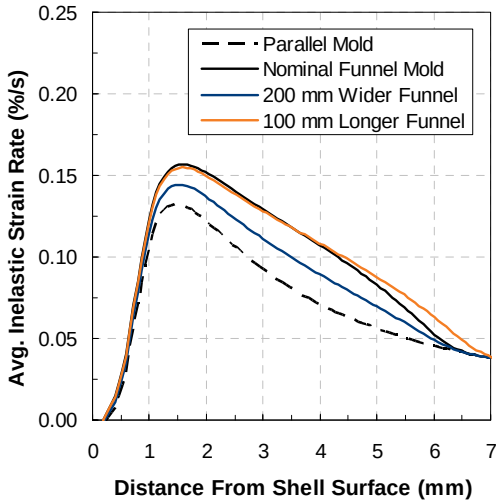

Figure 19. Avg. Inelastic Strain Rate in BTZ

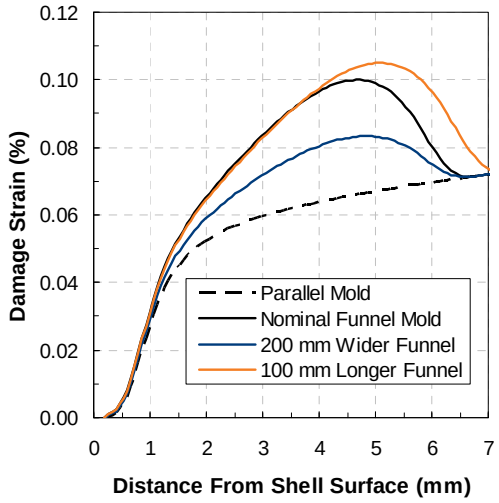

Figure 20. Accumulated Damage Strain in BTZ

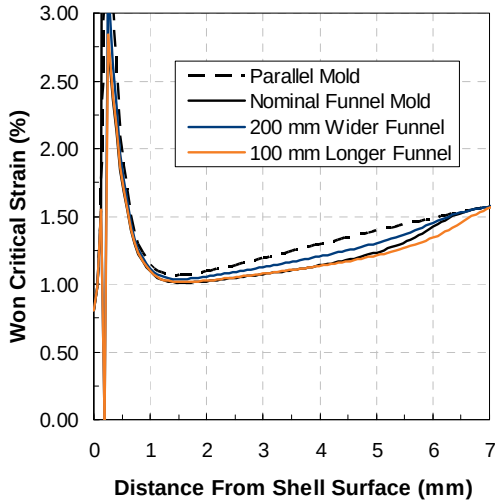

Figure 21. Won Critical Damage Strain

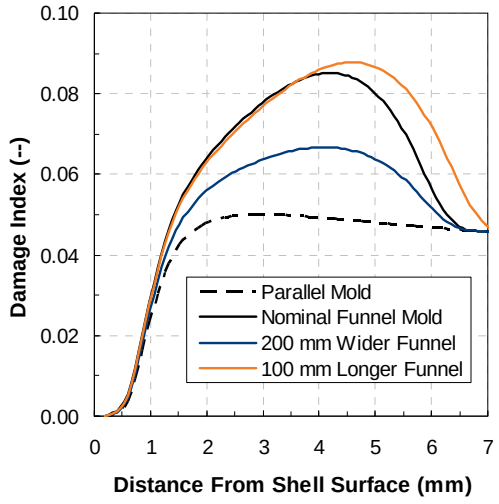

Figure 22. Damage Index

Increasing the width of the funnel, or more importantly the horizontal funnel radius, decreases the cracking potential caused by the funnel. Using a longer funnel slightly decreases the damage at points just below the surface, but increases it at points deeper beneath the surface; this is due to the wider mushy zone collecting more damage.

6. CONCLUSIONS

A simple analytical model (Equation (1)) has been developed that quantitatively describes the bending strain induced in the solidifying steel shell by interaction with funnel mold walls. This simple model has been shown to be surprisingly accurate when compared with the results of a two-dimensional, elastic-viscoplastic coupled thermal-stress finite element model. The model shows that bending strain is

inversely proportional to the horizontal radius of curvature of the funnel mold. Thus, a larger funnel radius is better and can be achieved by increasing outer funnel width, decreasing inner funnel width, and/or decreasing crown. Increasing the funnel length is another method of reducing the strain rate, but this may have negative repercussions on hot-tear crack formation. The potential of hot-tear crack formation was evaluated for funnel molds with the Won damage model by coupling the simple analytical model with a one-dimensional finite-element model of the solidifying shell. Under normal operation, funnel molds do not cause cracks though they do make the shell slightly more sensitive to crack formation. This can be reduced following the same guidelines just mentioned; a more gentle funnel (larger radius) is less susceptible to forming hot-tear cracks.

7. REFERENCES

1. R.C. Hibbeler, *Mechanics of Materials*, 5e. Prentice Hall, Upper Saddle River, New Jersey, (2003).
2. A.C. Ugural and S.K. Fenster, *Advanced Strength and Applied Elasticity*, 4e. Prentice Hall, Upper Saddle River, New Jersey, (2003).
3. H. Mizukami, K. Murakami, and Y. Miyashita, “Elastic Modulus of Steels at High Temperature.” *Tetsu-to-Hagané*, **63** (1977), pg. S-652.
4. Y.-M. Won, T.-J. Yeo, D. J. Seol, and K. H. Oh, “A New Criterion for Internal Crack Formation in Continuously Cast Steels.” *Metallurgical and Materials Transactions*, **31B** (2000), No. 4, pg. 779-794.
5. C. Li and B.G. Thomas, "Maximum Casting Speed for Continuous Cast Steel Billets Based on Sub-Mold Bulging Computation," in Steelmaking Conf. Proc., Vol. 85, ISS, Warrendale, PA, (Nashville, TN, March 10-13, 2002), 2002, 109-130.